#511276

Sandia National Laboratories
Operated for the U.S. Department of Energy by
Sandia Corporation

Albuquerque, New Mexico 87185-1328

date: November 2, 1999

to: Melvin Marietta, 6821

from: Teklu Hadgu, 6821, Palmer Vaughn, 6821, Jim Bean, 6849, Donna Johnson, 6848, Jay Johnson, 6849, Kathy Aragon, 6821, Jon Helton, 6849.

subject: Modifications to the 96 CCA direct brine release calculations

Memo Summary:

Re-runs were made of the 1996 CCA direct brine release (DBR) calculations with some changes. Corrective action was required in amending the equation for productivity index and modifying the model for abandoned wells (for intrusion scenarios). The corrections made are described below.

Corrections to productivity index: A study of well productivity index derivations shows that Eq. 2.2 in Section 2 of the attached report needs to be modified. A factor of 2π is missing, which may have resulted from translation of an equation based on petroleum units into S.I. units. An analysis of the case is given in Section 2.

Modifications to the model for abandoned wells: The 1996 CCA DBR analysis includes calculations for a second drilling intrusion that has been preceded by an intrusion into the repository and brine pocket. The first intrusion (now considered an abandoned well) is represented in the DBR simulations by using calculated values of a wellbore pressure and a productivity index in the input of BRAGFLO. The calculations for the wellbore pressure assumed that flow from a hypothetical brine pocket into the repository via the abandoned well directly enters the second intrusion borehole. Details of the method used can be found in Helton et al, (1998). Improvements were made to model the abandoned borehole without direct coupling to the second drilling intrusion borehole. This assumes that any flow between the boreholes is to be treated as flow in porous media. A new model for abandoned wells is given in Section 5.

The above changes were incorporated in the input to Pre-ALGEBRA, and the 96 CCA DBR runs were repeated for one replicate (5200 calculations). These changes resulted in some increment in brine release rates. However, these increases were not significant enough to adversely impact compliance.

Details of the new calculations and comparisons of results with those of the 96 CCA are given in the attached report.

WIPP:1.2.07.02.01:CO/CCA:QA: Modifications to the 96 CCA

Modifications to the 96 CCA Direct Brine Release Analysis

1. Introduction

This report deals with work done to correct, improve and reproduce methodology that was implemented in the 1996 Compliance Certificate Application (CCA) calculations on direct brine release (Helton et al., 1998, Stoelzel and O'Brien, 1996). Direct brine release (DBR), the subject of this study, is the release of contaminated brine to the accessible environment due to inadvertent borehole intrusion into the repository. In the 96 CCA DBR analysis brine release rates were calculated using BRAGFLO, and curve fits for flowing bottomhole pressure (FBHP). The curve fits represent an indirect coupling of the borehole and repository. The FBHP data to generate the curve fits were obtained using an iterative procedure involving Poettmann-Carpenter (1952) two-phase flow correlations for vertical flow in a borehole. The procedure used to generate the FBHP data can be summarized as follows:

- Set randomly generated repository properties (i.e. panel pressure, saturation, etc).
- Assume a value of FBHP.
- Calculate phase productivity indexes and flow rates using Eqs. 2.2 and 2.1 in Section 2 respectively.
- Calculate pressure drop up the borehole using Poettmann-Carpenter correlations.
- Iterate on FBHP until calculated wellhead pressure is within an error limit of a selected wellhead pressure (1 atm.).

As stated in the Memo Summary, this study involves correcting the equation used in the 96 CCA for productivity index, and improving the model for abandoned wells (for disturbed scenarios). Eq. 2.2 in Section 2 below needs to be modified to include a factor of 2π. This however, would affect the curve fits for FBHP as the procedure to generate the FBHP data involves productivity index. Sections 2 to 4 describe the changes made and the work involved in constructing new FBHP curve fits. In Section 4 the new curve fits are compared with those of the 96 CCA. Section 5 describes the new model for abandoned wells for two cases: an open hole and a sand filled well.

The above changes were incorporated into the DBR calculations through the inputs to Pre-ALGEBRA. The new FBHP curve fits and the new model for abandoned wells (for disturbed Scenarios with an abandoned well) were included in the Pre-ALGEBRA input files. Note that this procedure did not include code modifications either in BRAGFLO or its pre- and post-processors. The new DBR calculations were made in CMS in exactly the same way as the 96 CCA. CCDF calculations were also made to verify that the direct releases were still within the limits set by the EPA. The results of the new runs together with comparisons with the 96 CCA are given in Section 6.

2. Deliverability Method for Direct brine Release Analysis

2.1 Productivity Index for Radial Flow into a Well

In the preparation of the look-up table for FBHP in the DBR analysis (for the 96 CCA), the following two-phase equations were used:

$$q_p = J_p(P_p - P_{wf}) \tag{2.1}$$

where: P_p = repository pressure
P_{wf} = flowing bottomhole pressure
q_p = phase volume flowrate.
J_p = phase productivity index

The phase productivity index was defined as:

$$J_p = \frac{kk_{rp}h}{\mu_p\left[\ln\left(\frac{r_e}{r_w}\right) + s - 0.5\right]} \tag{2.2}$$

where: k = intrinsic permeability
k_{rp} = phase residual saturation
r_e = equivalent radius of grid block containing intrusion borehole
r_w = well radius
h = crushed panel height
μ_p = phase viscosity
s = skin factor

The literature also includes use of the productivity index PI, which using Eq. 2.1, is related to the phase productivity index as:

$$PI = \frac{J_P\mu_P}{k_{rp}} \tag{2.3}$$

Thus, using Eqs. 2.2 and 2.3, PI is expressed as:

$$PI = \frac{kh}{\ln\left(\frac{r_e}{r_w}\right) + s - 0.5} \tag{2.4}$$

The Sandia Report SAND98-0365 (1998) attributes Eq. 2.2 to the references Mattax and Dalton (1990), Williamson and Chappelear (1981a), Williamson and Chappelear (1981b). The publication by Hadgu et al. (1995) also has a similar analysis on well deliverability. These publications all give the productivity index as:

$$PI = \frac{2\pi kh}{\ln\left(\frac{r_e}{r_w}\right) + s - 0.5} \tag{2.5}$$

Note that some of the references exclude skin factor and the factor for steady-state flow (i.e. – 0.5). Comparing Eq. 2.4 and 2.5 a difference of 2π exists. If Eqs. 2.4 and 2.5 are both based on a representation of radial flow into a well, then Eq. 2.5 seems to be the appropriate equation, and hence all

previous calculations have to be multiplied by a factor of 2π. Following is a derivation of Eq. 2.5 using Darcy's law.

2.2 Radial Flow into a Well for Single-Phase Flow

Darcy flow in radial direction is given as:

$$q = \frac{kA}{\mu}\frac{dP}{dr} \tag{2.6}$$

where the flow area A in cylindrical coordinates is: $A = 2\pi rh$. Substituting the definition of A into Eq. 2.6 results in:

$$q = \frac{2\pi rhk}{\mu}\frac{dP}{dr} \tag{2.7}$$

Separating variables in Eq. 2.7 and integrating (for r in the range of $r_w - r_e$ and for P in the range of $P_w - P_e$):

$$\frac{q}{2\pi h}\int_{r_w}^{r_e}\frac{dr}{r} = \frac{k}{\mu}\int_{P_{wf}}^{P_e} dP \tag{2.8}$$

where P_e = pressure at external boundary
P_w = pressure at well
r_e = radius at external boundary
r_w = well radius
h = thickness of completion interval

After integration:

$$q = \frac{2\pi kh(P_e - P_{wf})}{\mu \ln(r_e / r_w)} \tag{2.9}$$

Eq. 2.9 can also be written as:

$$q = PI(P_e - P_{wf})/\mu \tag{2.10}$$

The productivity index PI is then:

$$PI = \frac{2\pi kh}{\ln(r_e / r_w)} \tag{2.11}$$

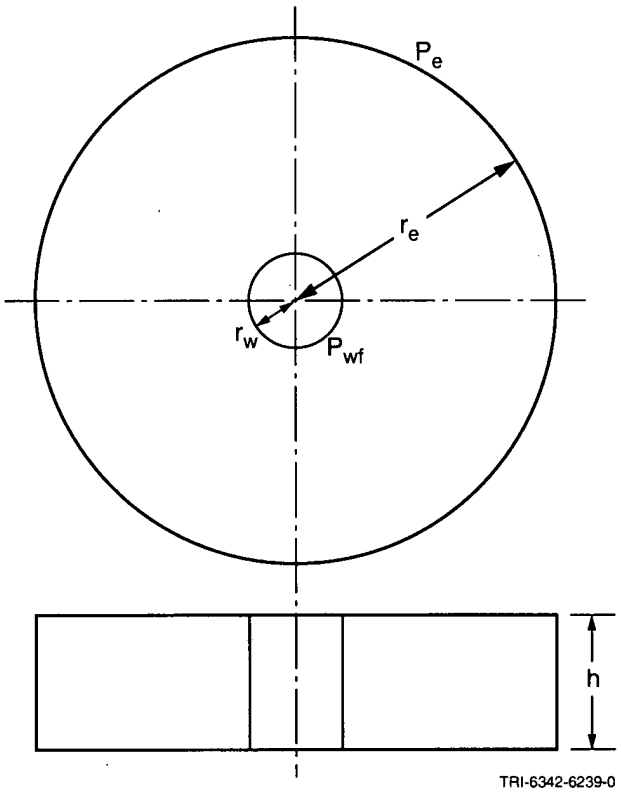

Fig. 1. Schematic diagram for radial flow into a well

3. Use of Poettmann-Carpenter Two-Phase Flow Pressure Drop Correlations

To evaluate pressure drop in the intrusion borehole as repository fluid flows to the surface the Poettmann-Carpenter method (Poettmann and Carpenter 1952, Welchon et al. 1962) was used for the 1996 CCA calculations. The method was selected because some of the data used in developing the correlations included flow through the annulus of two-pipes, and also because the method is relatively easy to implement. The method was designed to evaluate pressure drop of liquid (oil and water) and gas in oil wells.

Main assumptions of the method:

- Homogeneous steady gas-liquid flow.
- Pressure loss due to viscous shear is negligible. Only the numerator of the Reynolds number is used in correlating friction factor (i.e. viscosity not included). This was attributed to the turbulet flow of a flowing oil well.
- Friction factor correlation based on 2 – 3 inch tubing.

To evaluate FBHP for WIPP applications the Poettmann-Carpenter method was used with some modifications. In the original Poettmann-Carpenter method oil was the primary fluid and petroleum industry units were used in the pressure drop equations. Parameters were defined in terms of barrels of stock-tank oil. Thus, references to oil have been changed to that of brine for WIPP-related calculations. The liquid phase is now represented by brine (instead of oil and water), and the gas phase is represented

by hydrogen (instead of petroleum gases). Note that since brine has replaced oil, any references to water have been removed. With these modifications the pressure gradient for flow in an annulus is given by:

$$\frac{dP}{dh} = \frac{M}{144V_m}\left(1 + \frac{f'Q_b^2V_m^2}{7.413x10^{10}(D_i - D_o)^3(D_i + D_o)^2}\right) \tag{3.1}$$

where:

$\frac{dP}{dh}$ = pressure gradient in (psi/ft)
P = absolute pressure (psia)
h = depth (ft)
V_m = Volume of mixed gas and brine at pressure P per barrel of stock-tank liquid (i.e. brine), based on the ratio of fluids flowing into and out of the flow string.

$$V_m = 5.615B_w + \frac{P_{st}T_aZ}{PT_{st}}R_p \tag{3.2}$$

P_{st} = base pressure at which gas is measured (14.7 psia)
T_{st} = base temperature at which gas is measured (540.27 °R)
T_a = average temperature of flow (540.27 °R)
B_w = formation volume factor of water = 1
Z_g = compressibility factor of the gas (hydrogen) at temperature T_a and pressure P. For a constant temperature of 540.27 °R (27 °C) the report SAND98-0365 (Helton et al., 1998) gives:
Z = 1 + P x 5.88966 x 10^{-4} , where P is pressure in psia.
R_p = producing gas liquid ratio (cubic ft per bbl stock-tank liquid)
V_b = cubic ft of brine produced per bbl stock-tank liquid
M = total mass of gas and brine, lb, associated with 1 bbl stock-tank liquid flowing into and out of the flow string.

$$M = (5.615)(62.4)\gamma_b + 0.0764\gamma_g R_p \tag{3.3}$$

γ_g = gas (hydrogen) gravity =2.02/28.96
γ_b = specific gravity of brine =1.23
Q_b = bbl of stock-tank liquid produced per day (bbl/day)
D_i = Inside diameter of casing or open-hole (ft)
D_o = outside diameter of tubing (ft)
f' = Poettmann-Carpenter friction factor

Poettmann and Carpenter correlated data of flowing oil and gas-lift wells using an integrated form of Eq. 3.1 to evaluate the friction factor f'. The friction factor was correlated as a function of the numerator of Reynolds number, ignoring viscosity:

$$Dv\rho = 1.4737x10^{-5}\frac{Q_b M}{(D_i + D_o)} \qquad (3.4)$$

where: D = diameter
v = fluid velocity
ρ = fluid density

Note that in the pressure gradient equation (Eq. 3.1) the term $(D_i - D_o)^3 (D_i + D_o)^2$ replaces D^5 for flow in an annulus between two pipes. Also, the term $(D_i + D_o)$ was used instead of D in Eq. 3.4 for flow in an annulus. Poettmann and Carpenter (1952) presented a plot of f' against $Dv\rho$ (given by Eq. 3.4) for flowing and gas-lift wells. Stoelzel and O'Brien (1996) provided a curve fit of the plot given by:

$$f' = a + \frac{b}{x} + \frac{c}{x^2} + \frac{d}{x^3} + \frac{e}{x^4} + \frac{f}{x^5} \qquad (3.5)$$

where: x = Dvρ in Eq. 3.4; and the coefficients are:
a = 0.0034152139
b = 0.05040896
c = 3.8265844
d = 8.0204911
e = 62.225962
f = 24.126862

4. Preparation of FBHP "Look-Up" Table and Curve Fits

To obtain dynamic FBHP the available options are a direct coupling of the vertical two-phase flow code (i.e. Poettmann-Carpenter) and the reservoir code (i.e. BRAGFLO), or use of a prepared "look-up" table together with BRAGFLO. In this study the "look-up" table approach has been used in line with the 96 CCA calculations. Following is a description of the approach.

Due to the changes made to the productivity index equation (Eq. 2.4 vs. Eq. 2.5), FBHP curve fits from the 96 CCA are no longer applicable. Thus new curve fits that reflect the changes had to be made. In obtaining the curve fits a similar procedure as in the 96 CCA was used. Terminology used in the 96 CCA calculations was also adopted. Three curve fits representing brine only flow (i.e. $k_{rg} = 0$), brine dominated flow (i.e. $k_{rw} > k_{rg}$) and gas dominated flow ($k_{rg} > k_{rw}$) were considered. In the 96 CCA calculations the three curve fits represented FBHP over the three flow regimes (as a function of two parameters): .

Brine only flow:

$$FBHP = f(J_b, P_r) \quad \text{for } k_{rg} = 0 \qquad (4.1)$$

Brine dominated flow:

$$FBHP = f(log(k_{rg}/k_{rw}), P_r) \qquad \text{for } \log(k_{rg}/k_{rw}) < 0 \tag{4.2}$$

Gas dominated flow:

$$FBHP = f(log(k_{rg}/k_{rw}), P_r) \qquad \text{for } \log(k_{rg}/k_{rw}) > 0 \tag{4.3}$$

The current study looked at various parameters to investigate best representation of FBHP. In theory Eqs. 2.1 and 2.2 show that FBHP is a function of several repository variables. In a vector form the variables are:

$$\mathbf{v} = (k, P_r, S_w, S_{wr}, S_{gr}, s, h) \tag{4.4}$$

The relative importance of these variables varies. The study looked at how the curve fits could be representative of these variables. In the 96 CCA calculations permeability was kept constant, and thus, it can be removed from the vector. Brine saturation and the residual saturations can be represented by relative permeabilities, as was also done in the 96 CCA. These and other ideas were used in finding curve fits for the modified FBHP. Various combinations of the variables in Eq. 4 were applied to obtain good fits to the new FBHP data. Better accuracy was obtained with curve fits for FBHP as a function of the following parameters:

Brine only flow:

$$FBHP = f(J_b, P_r) \qquad \text{for } k_{rg} = 0 \tag{4.5}$$

Brine dominated flow:

$$FBHP = f(log(k_{rg}/k_{rw}), P_r) \qquad \text{for } \log(k_{rg}/k_{rw}) < 0 \tag{4.6}$$

Gas dominated flow:

$$FBHP = f(J_g, P_r) \qquad \text{for } \log(k_{rg}/k_{rw}) > 0 \tag{4.7}$$

Note that only the relationship for gas dominated flow (Eq. 4.7) is different from those of the 96 CCA. For brine dominated flow FBHP was found to be a strong function of pressure, and the effect of skin factor and crushed panel height was minimal. However, for gas dominated flow the effect of the variables skin factor and crushed panel height was more pronounced. In the 96 CCA analysis the FBHP curve fits were constructed using randomly generated values of the parameters shown in Eq. 4.4 with the exception of permeability. For this study, however, actual data from the 96 CCA 10,000 runs were used to construct the FBHP curve fits. This would improve the accuracy of the curve fits as will be discussed subsequently. A FORTRAN program "fbhp99modified.for" was written to obtain flowing bottomhole pressure data to prepare the FBHP "look-up" table or curve fits. Note that the new FBHP values reflect

corrections made to the productivity index equation. To prepare the calculations for FBHP the following values were first assigned for constant parameters.

k = waste permeability = 1.7×10^{-12} m^2
T = temperature = 300.1 °K
P_{wh} = wellhead pressure = 1 atm.
P_{st} = base pressure at which gas is measured (for Poettmann-Carpenter calculations) = 1 atm.
γ_b = specific gravity of brine = 1.23
γ_g = gas (hydrogen) gravity = 2.02/28.96
B_w = formation volume factor of brine = 1.0
μ_b = viscosity of brine = 1.8×10^{-3} Pa·s
μ_g = viscosity of gas 8.92×10^{-6} Pa·s
r_e = external drainage radius = 10.2 m
r_w = wellbore radius = 0.1556 m
c = constant for pseudo steady-state flow = -0.50
Repository depth = 655.32 m
Depth discretization increment for Poettmann-Carpenter calculations = 7.62 m (25 ft)

Well geometry used (based on current drilling practices in the area):

Surface to 182.88 m: surface casing with ID = 0.323 m
182.88 b to 655.32 m: open hole with 0.3112 m diameter

Drill string consisting of:

Surface to 472.44 m: drill pipe with OD = 0.0889 m
472.44 m to 655.32 m: drill collar with OD = 0.2032 m

Relative permeabilities were calculated using relative permeability curves of Brooks-Corey: original wetting phase, modified non-wetting phase (BRAGFLO input parameter KRP = 4).

The iterative process for the evaluation of FBHP solves the problem:

$$P_{whcalc}(FBHP) - P_{wh} = 0 \qquad (4.8)$$

where: P_{wh} = specified wellhead pressure (1 atm.)
P_{whcalc} = calculated wellhead pressure

An initial value of FBHP is first selected to start the iteration. Eq. 2.1 is then used to evaluate phase flowrates. Next the Poettmann-Carpenter method is applied to calculate pressure drop up the annulus of the borehole to obtain wellhead pressure. Iterations continue until the difference between the calculated wellhead pressure and the selected wellhead pressure (i.e. the error) approaches zero. The error is calculated from:

$$error = \frac{(P_{whcalc} - P_{wh})}{P_{wh}} x100\% \qquad (4.9)$$

Small increments of FBHP were taken until the error changed sign (i.e. the zero was bracketed) and then the Bisection method was used to find the zero. The steps followed are given below.

1. Obtain values of P_r,S_w,S_{wr},S_{gr},s,h
2. Calculate phase productivity indices using Eq. 2.2.
3. Select FBHP
4. Evaluate phase flowrates using Eq. 2.1.
5. Use Poettman-Carpenter method to calculate up the intrusion borehole to evaluate wellhead pressure (P_{whcalc}).
6. Calculate the error given by Eq. 4.9.
7. Continue with FBHP increments until the error changes sign (i.e. the zero is bracketed).
8. Use Bisection method to reduce the error to a selected value (i.e. find the zero). This would provide the FBHP for the selected repository parameters.
9. Continue calculating FBHP values for other repository parameters using the random number generator.

Three tables were then generated using the calculated values of FBHP as functions of the variables discussed above. The commercial code "TableCurve 3D" was then used to produce curve fits to the "look-up" tables. The resulting curve fit equations are as shown below.

<u>For brine only flow(k_{rg}=0):</u>

$$FBHP = a + bx + cy + dx^2 + ey^2 + fxy + gx^3 + hy^3 + ixy^2 + jx^2y \qquad (4.10)$$

where $x = \log(J_b)$ and $y = P_r$(= panel pressure).

The coefficients are:

a = 3.2279346×10^{11}
b = 9.4816648×10^{10}
c = -6.2002715×10^{3}
d = 9.2450601×10^{9}
e = 4.1464475×10^{-6}
f = -1.2886068×10^{3}
g = 2.9905582×10^{8}
h = $1.0857041 \times 10^{-14}$
i = 4.7119798×10^{-7}
j = -66.90712

With resulting coefficient of determination $R^2 = 0.974$

<u>For brine dominated flow ($k_{rw} > k_{rg}$):</u>

$$FBHP = \frac{a + bx + cx^2 + dy}{1 + ex + fx^2 + gx^3 + hy} \qquad (4.11)$$

where $x = \log(k_{rg}/k_{rw})$ and $y = P_r$(= panel pressure).

The coefficients are:

a $= 1.6065077 \times 10^{6}$
b $= 2.6243397 \times 10^{6}$
c $= 2.4768899 \times 10^{6}$
d $= -5.3635476 \times 10^{-2}$
e $= 7.0815693 \times 10^{-1}$
f $= 3.8012696 \times 10^{-1}$
g $= 4.1916956 \times 10^{-3}$
h $= -2.4887085 \times 10^{-8}$

With resulting coefficient of determination $R^2 = 0.997$

For gas dominated flow ($k_{rg} > k_{rw}$):

$$FBHP = a + b/x + cy + d/x^2 + ey^2 + fy/x + g/x^3 + hy^3 + iy^2/x + jy/x^2 \qquad (4.12)$$

where $x = \log(J_g)$ and $y = P_r$(= panel pressure).

The coefficients are:

a $= -1.0098405 \times 10^{9}$
b $= -2.3044622 \times 10^{10}$
c $= 9.8039146$
d $= -1.7426466 \times 10^{11}$
e $= 1.8309137 \times 10^{-7}$
f $= 1.7497064 \times 10^{2}$
g $= -4.3698224 \times 10^{11}$
h $= -1.4891198 \times 10^{-16}$
i $= 1.3006196 \times 10^{-6}$
j $= 7.5744833 \times 10^{2}$

With resulting coefficient of determination $R^2 = 0.949$

Note that though these curve fit equations are overall relatively accurate (as indicated by the R^2 values), individual points can be inaccurate. Thus care should be exercised in using the equations. Figs. 4.1 to 4.3 show the accuracy of these curves by comparing FBHP values with those calculated using Poettmann-Carpenter correlations. Figs. 4.4 to 4.6 show accuracy of the curves used in the 96 CCA. For brine dominated flow the curve fits are not very accurate at low pressures (Figs. 4.2 and 4.5). For gas dominated flow Figs. 4.3 and 4.6 show noticeable scatter. Direct use of FBHP values from Poettmann-Carpenter correlations would alleviate the problem, but that is a subject of a future study. Note that in obtaining the new FBHP curve fits the same procedure has been used as in the 96 CCA. The functional forms of the selected equations for fitting FBHP were based on the optimum values of R^2 and computational efficiency in the code implementation of the equations.

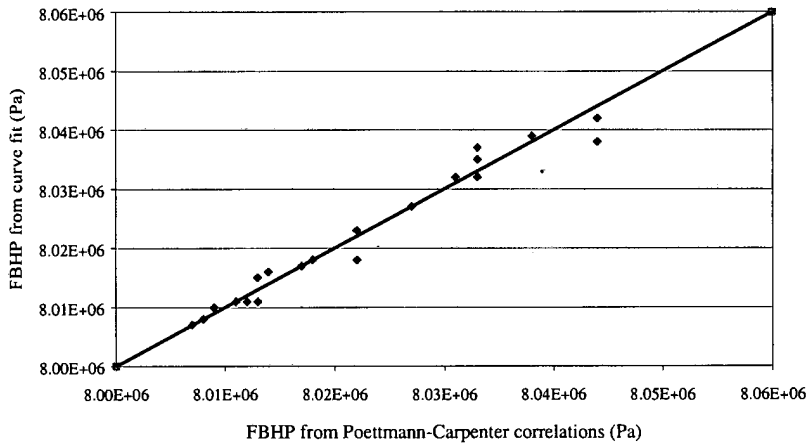

Fig. 4.1 Comparison of FBHP predictions from new curve fits and Poettmann-Carpenter correlations for brine only flow ($k_{rg} = 0$).

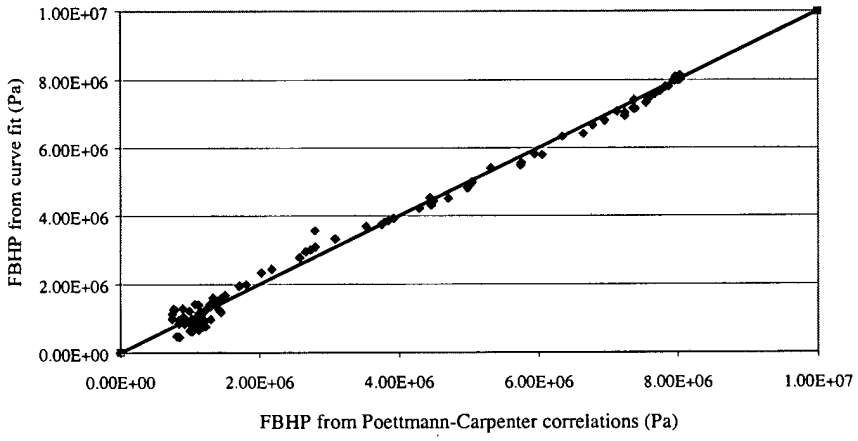

Fig. 4.2 Comparison of FBHP predictions from new curve fits and Poettmann-Carpenter correlations for brine dominated flow ($k_{rw} > k_{rg}$).

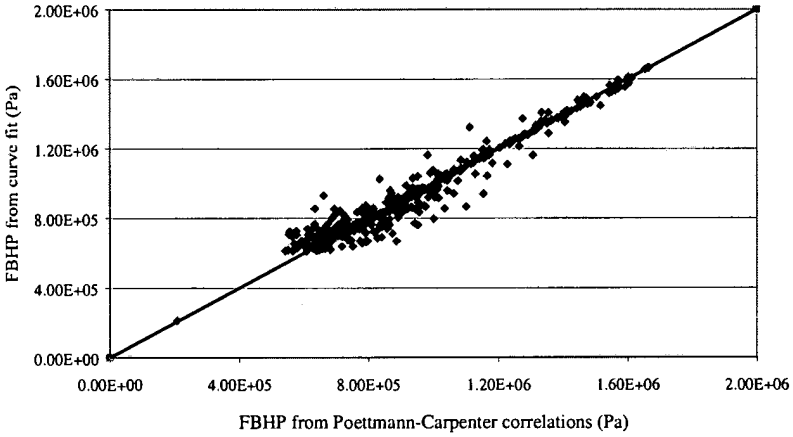

Fig. 4.3 Comparison of FBHP predictions from new curve fits and Poettmann-Carpenter correlations for gas dominated flow ($k_{rg} > k_{rw}$).

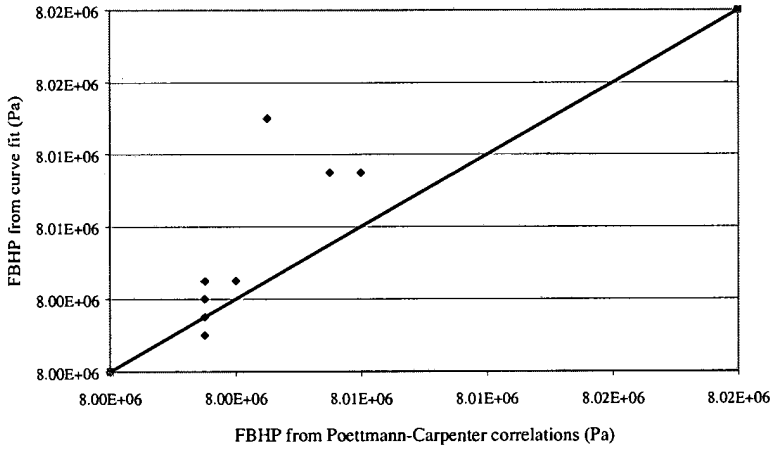

Fig. 4.4 Comparison of FBHP predictions from 96 CCA curve fits and Poettmann-Carpenter correlations for brine only flow ($k_{rg} = 0$).

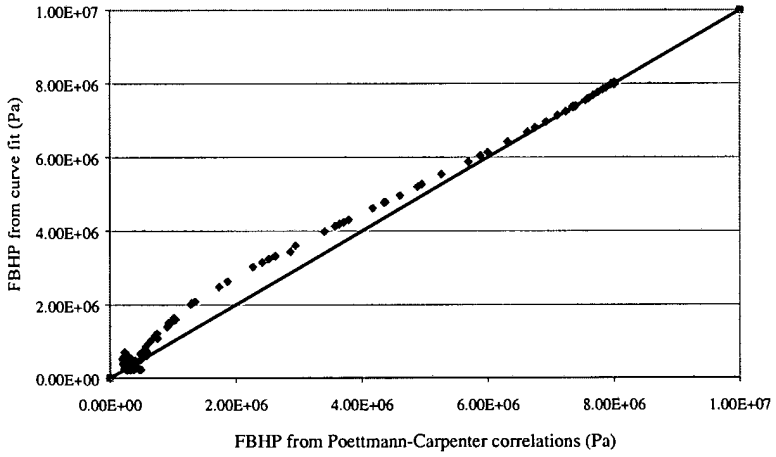

Fig. 4.5 Comparison of FBHP predictions from 96 CCA curve fits and Poettmann-Carpenter correlations for brine dominated flow ($k_{rw} > k_{rg}$).

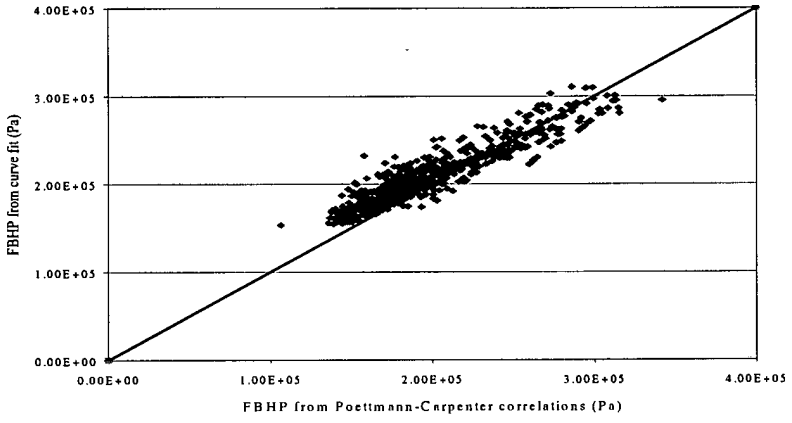

Fig. 4.6 Comparison of FBHP predictions from 96 CCA curve fits and Poettmann-Carpenter correlations for gas dominated flow ($k_{rg} > k_{rw}$).

5. Boundary condition from Previous Intrusions

Direct brine release is also affected by the presence of abandoned wells from previous intrusions into the repository. Some of the DBR calculations account for previous intrusions striking a hypothetical brine pocket located below the repository. Brine flow from the brine pocket to the repository through abandoned boreholes is accounted for using boundary conditions. This is handled by specifying a productivity index and a flowing bottomhole pressure at grid blocks containing the abandoned boreholes. More information on previous intrusions can be found in Section 4.7.6 of Helton et al. (1998).

Two possibilities have been considered for the borehole between the brine pocket and the repository: (1) an open borehole, and (2) a borehole filled with porous material (with properties similar to silty sand). The first case corresponds to the situation in which the drilling intrusion under consideration occurs within 200 years of a previous drilling intrusion that penetrated the pressurized brine pocket. The second case corresponds to the situation in which the drilling intrusion under consideration has occurred more than 200 years after a previous drilling intrusion that penetrated the brine pocket. Following is an analysis to obtain representative boundary conditions for the brine pocket.

5.1 Case 1: Open Hole

Flow from the pressurized brine pocket to an abandoned borehole can be represented by the familiar deliverability equations described in Section 2 above. Using brine pocket parameters:

$$q_{BP} = \frac{PI_{BP}\left(P_{BP} - P_{wfBP}\right)}{\mu_b} \tag{5.1}$$

and

$$PI_{BP} = \frac{2\pi k_{BP} h_{BP}}{\ln\left[\frac{re_{BP}}{r_w}\right] - 0.5} \tag{5.2}$$

where BP indicates brine pocket. Note that skin effect has been neglected in Eq. 5.2. Assuming an open hole between the brine pocket and the repository, vertical flow of brine in the borehole is a function of frictional and gravitational pressure drops. It is further assumed that for laminar flow of brine in the borehole friction is negligible compared to the gravitational pressure drop. Thus, the difference in pressure between the bottom and top of the borehole can be given as:

$$P_{wfBP} - P_{wfBC} = \rho_b g L_{BP} \tag{5.3}$$

where: P_{wfBC} = flowing pressure of boundary condition at repository
ρ_b = brine density
g = acceleration due to gravity
L_{BP} = Distance from brine pocket to repository (i.e. length of the abandoned borehole)

Flow from the abandoned borehole to the repository can also be represented by the deliverability equations described in Section 2. Using boundary condition parameters:

$$q_{BC} = \frac{PI_{BC}\left(P_{wfBC} - P_{BC}\right)}{\mu_b} \tag{5.4}$$

$$PI_{BC} = \frac{2\pi k_{BC} h_{BC}}{\ln\left[\frac{re_{BC}}{r_w}\right] - 0.5} \tag{5.5}$$

where BC indicates boundary condition in the repository grid block. The sign of the pressure draw down in Eq. 5.4 is reversed from that of Eq. 2.1 so that positive flow represents flow into the repository. Note that skin effect has also been neglected in Eq. 5.5. Combining Eqs. 5.1, 5.3 and 5.5, and assuming that $q_{BP} = q_{BC}$ an expression for the well flow rate as a function of P_{BP} and P_{BC} is:

$$q_{BC} = \frac{P_{BP} - \rho_b g L_{BP} - P_{BC}}{\mu_b\left[\frac{1}{PI_{BC}} + \frac{1}{PI_{BP}}\right]} \tag{5.6}$$

Thus, the brine injection flowrate from brine pocket to the repository can be obtained using brine pocket pressure and repository pressure in the grid block containing the abandoned borehole. To change Eq. 5.6 into the form used in BRAGFLO (Eq. 5.7), equivalent parameters are defined as follows. Eq. 5.6 is replaced by Eq. 5.7:

$$q_{BC} = \frac{PI_{BC}^{equiv}}{\mu_b}\left[P_{wfBC}^{equiv} - P_{BC}\right] \tag{5.7}$$

where the equivalent boundary condition productivity index and flowing bottomhole pressure are defined as:

$$P_{wfBC}^{equiv} = P_{BP} - \rho_b g L_{BP} \tag{5.8}$$

$$PI_{BC}^{equiv} = \frac{1}{\frac{1}{PI_{BC}} + \frac{1}{PI_{BP}}} \tag{5.9}$$

Eqs. 5.8 and 5.9 are then used to calculate the equivalent parameters to be used in BRAGFLO. Since the DBR grid does not explicitly model the brine pocket, it is represented by the boundary condition defined by these parameters.

5.2 Case 2: Sand Filled

As with Case 1 flow from the pressurized brine pocket to an abandoned borehole can be represented by Eqs. 5.1 and 5.2. In Case 2 the abandoned borehole between the brine pocket and the repository is filled with porous medium material. The vertical flow of brine is then represented by Darcy flow as:

$$q_{BP} = \frac{K_{BH} A_{BH}}{\mu_b L_{BP}} \left[P_{wfBP} - P_{wfBC} - \rho_b g L_{BP} \right] \tag{5.10}$$

where K_{BH} = borehole permeability
A_{BH} = borehole flow area = $\pi D^2/4$

Combining Eqs. 5.1, 5.5 and 5.10 and assuming that $q_{BP} = q_{BC}$ an expression for q_{BC} as a function of P_{BP} and P_{BC} is obtained as shown below.

$$q_{BC} = \frac{P_{BP} - \rho_b g L_{BP} - P_{BC}}{\mu_b \left[\frac{1}{PI_{BC}} + \frac{1}{PI_{BP}} + \frac{L_{BP}}{K_{BH} A_{BH}} \right]} \tag{5.11}$$

Eq. 5.11 is similar to Eq. 5.9 with borehole properties included. As with Case 1, Eq. 5.11 can be transformed into a form used by BRAGFLO (i.e. Eq. 5.7), using the following equivalent parameters.

$$P_{wfBC}^{equiv} = P_{BP} - \rho_b g L_{BP} \tag{5.8}$$

$$PI_{BC}^{equiv} = \frac{1}{\frac{1}{PI_{BC}} + \frac{1}{PI_{BP}} + \frac{L_{BP}}{K_{BH} A_{BH}}} \tag{5.12}$$

6. DBR Calculation Results

Modifying the productivity index equation had an effect on parameters such as FBHP and the amount of brine releases to a varying degree. The FBHP "look-up" table preparation detailed in Section 4 was based on a constant productivity index whose modification would directly affect the calculated FBHP values. The BRAGFLO_DBR calculations for brine release also use a constant productivity index, which when changed, affects the amount of brine volume removed. To verify that the modification of the productivity index and the new model for abandoned wells did not adversely affect the overall direct releases the 1996 CCA calculations were repeated with these modifications. New BRAGFLO_DBR runs were made in CMS for one replicate (5200 calculations). Changes were made in the input files to Pre-ALGEBRA to include the new FBHP curve fits and to change the model for

abandoned wells. Following is a discussion of the results of the new calculations with comparisons to the 96 CCA calculations.

6.1 Modifications impact on FBHP

As is evident from Eq. 2.1 and discussions in Section 4, changes in the productivity index would affect the FBHP solution. In this case the variables obtained from the 10,000–year BRAGFLO calculations (panel pressure, saturation, permeability, residual saturations) remain constant during the iterative process. Figs. 6.1 to 6.3 show plots of FBHPs obtained from curve fits, for both the 96 CCA and 99 modified methods. Fig. 6.1 compares FBHPs of the two methods for brine only flow. Although the 99 modified method shows slightly higher FBHP values, the differences are not significant. This is due to the fact that wellbore pressure drop for brine only flow is dominated by gravity, which is not affected by changes in flow rate. Fig. 6.2 is a plot for brine dominated flow. This case is also characterized by relatively higher brine saturations, which would mean that gravity is important in the pressure drop calculations. Thus, the FBHPs are similar for the two methods except at low FBHPs. Lower FBHP's are associated with lower brine saturations. With lower brine saturations (i.e. higher gas saturations) frictional and accelerational pressure drops, which are a function of flow rate, become more pronounced.

In Eq. 2.1 a higher productivity index would increase flow rate if all other variables remain constant. But the flow rate that can be accommodated by the borehole is limited. Thus, for low saturation cases the increase in productivity index is accompanied by an increase in FBHP. This is consistent with what is observed in Fig. 6.2 at low brine saturations, and more importantly in Fig. 6.3. Fig. 6.3 shows significant differences in FBHP values. In summary results of the 96 CCA showed that higher brine releases are associated with brine saturations of about 0.7, which is characteristic of brine dominated flow. Thus, as also shown in Fig. 6.2, changes in FBHP are not very significant for vectors with high DBR.

6.2 Modifications impact on panel pressure, saturation and brine removed

As stated above panel pressures and saturations obtained from the 10,000-year BRAGFLO calculations (at times of intrusion) did not change during the FBHP evaluation process. But they do change during the BRAGFLO_DBR calculations, as repository fluid is removed. Note that in this study the PI and FBHP for each realization remain constant for the duration of flow. The pressure and saturation at the times of intrusion fixes the FBHP for the duration of the intrusion event. In reality FBHP would vary as conditions in the panel change. To study these and other effects as a result of the correction to PI, we have selected a realization with a high DBR in the replicate. The selected vector and its initial conditions are:

Replicate 1, Scenario 2, Vector 46, Intrusion time = 2000 years
Initial down-dip panel pressure = 10.53 MPa; Initial down-dip brine saturation = 0.667
Initial brine relative permeability = 0.2226; Initial gas relative permeability = 0.0295

The above data would put this realization in brine dominated flow. The duration of flow for this realization in the BRAGFLO_DBR run was 11 days. Figs. 6.4 to 6.11 show calculation results for both the 96 CCA and the 99 modified cases for the same realization. Fig. 6.4 shows cumulative brine release for both methods for the duration of flow. The curves indicate that the brine removed for the 99

modified case is larger than for the 96 CCA. The brine removed after 11 days of flow for the 96 CCA and 99 modified methods were 32 m^3 and 53 m^3 respectively. Thus, for this vector the increase in productivity index by a factor of 2π did not translate into an equivalent increase in brine removed. This is related to the fact that the larger PI resulted in depleting the grid block containing the borehole at a faster rate, resulting in the lowering of both reservoir pressure and saturation, which in turn slowed the release rate. As shown in the equation below, lowering of both reservoir pressure and saturation reduces brine release.

$$q_b = \frac{PI \cdot k_{rl}(S_b)}{\mu_l}(P_r - FBHP)$$

Fig. 6.5 is the same plot as Fig. 6.4 but in a log-log scale. The plot shows that the factor of 2π is evident at small times when grid block pressure and saturation did not change. Fig. 6.6 and 6.7 show direct comparison of brine releases for the two methods (99 modified and 96 CCA) in different scales.

Figs. 6.8 to 6.11 show pressure and saturation profiles for the two methods for the duration of flow. Figs. 6.8 and 6.9 are plots of panel pressure and brine saturation vs. time for the 96 CCA and 99 modified cases. Both cases start with near constant pressure and saturation at low flows (i.e. small times). As the rate of brine release increases both cases show sharp drops in pressure and saturation. However, the drops for the 99 modified run are greater than for the 96 CCA. The same observations can also be made with Figs. 6.10 and 6.11, which show direct comparisons of pressure and saturation for the two methods.

6.3 Modifications impact on CCDF's

The study also looked at the influence of the changes made to the complementary cumulative distribution function (CCDF). CCDF calculations were made in the same way as in the 96 CCA. Plots of normalized releases and volume releases for the 1999 modified and 96 CCA calculations are given in Figs. 6.12 to 6.20. Figs. 6.12 and 6.13 show distributions of CCDFs for total and DBR (blowout) normalized releases. Note that the total normalized releases include contributions of cuttings, spallings and DBR. Note also that the new calculations did not affect the releases due to cuttings and spallings. The modifications made only affect DBR and total releases. As with those of the 96 CCA, the CCDFs of the 99 modified calculations fall further from the dashed line representing EPA limit (specified in 40 CFR 191.13a). Comparing the new DBR normalized releases with those of the 96 CCA the curves have shifted slightly to the right. However, they are well within the EPA limit and do not impact compliance. Figs. 6.14 and 6.15 show direct comparison of the two methods using mean values of normalized releases. The plot for the comparison of direct brine releases shows higher differences at low releases than at high releases. The plots in Fig. 6.15 verify that releases due to cuttings and spallings have not been affected by the modifications.

Fig. 6.16 shows distribution of CCDFs for volume releases to the accessible environment for the 99 modified calculations. The differences between the 96 CCA and the 1999 modified calculations are more visible here. Fig. 6.17 shows a comparison of direct releases from the 96 CCA and modified calculations. The brine volumes removed in the new runs are larger than those of the 96 CCA. Observations of individual realizations indicate that vectors with smaller brine releases showed up to an order of magnitude higher releases, while vectors with higher brine releases have about doubled the

cumulative releases of the 99 CCA. This is consistent with the findings of the realization with Vector 46. Note that large differences on small releases do not impact compliance.

Figs. 6.18 to 6.20 show plots for multiple intrusions. The comparison of CCDFs of normalized releases and volume removed for multiple intrusions was similar to that of the undisturbed cases discussed above. The effect to brine releases due to the changes made in the model for abandoned wells were not significant. This is because the contribution of the abandoned wells to brine releases was low even with the 96 CCA calculations.

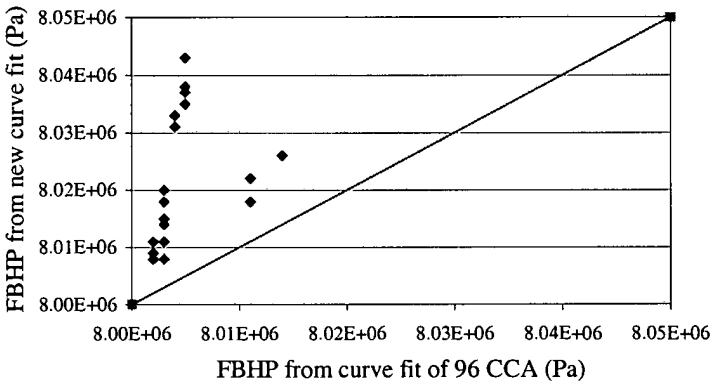

Fig. 6.1 Comparison of FBHP predictions using the 96 CCA and 99 new curve fits for brine only flow ($k_{rg} = 0$)

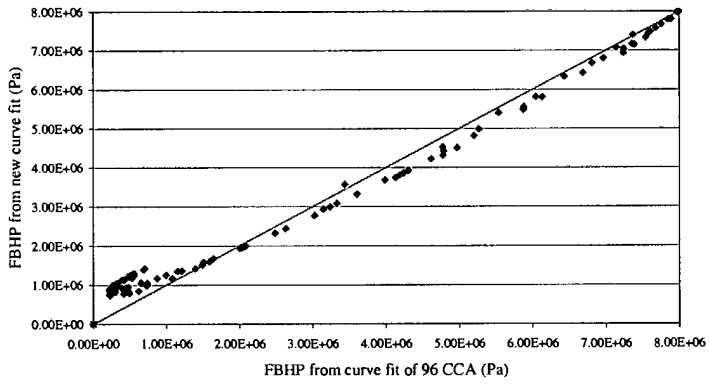

Fig. 6.2 Comparison of FBHP predictions using the 96 CCA and 99 new curve fits for brine dominated flow ($k_{rw} > k_{rg}$)

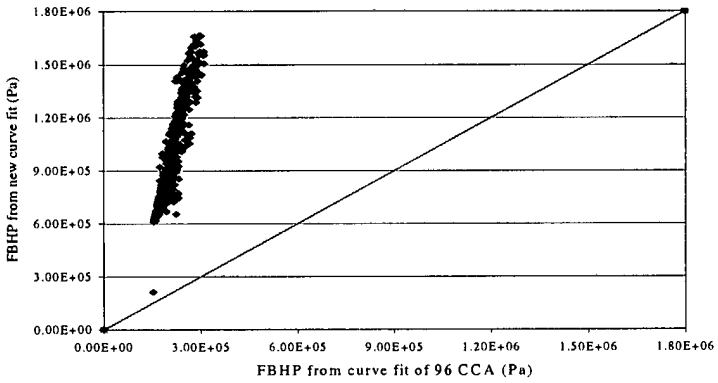

Fig. 6.3 Comparison of FBHP predictions using the 96 CCA and 99 new curve fits for gas dominated flow ($k_{rg} > k_{rw}$)

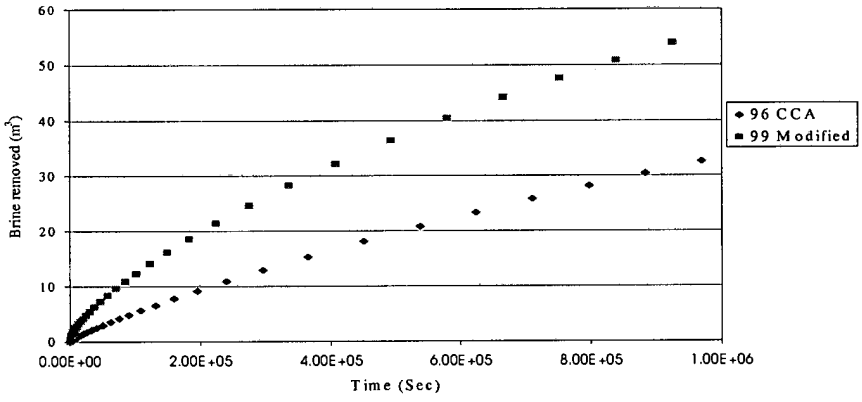

Fig. 6.4 Cumulative brine release vs. time predictions for both the 96 CCA and 99 modified calculations. (Down-dip, Replicate 1, Vector 46, Intrusion time 2000 years)

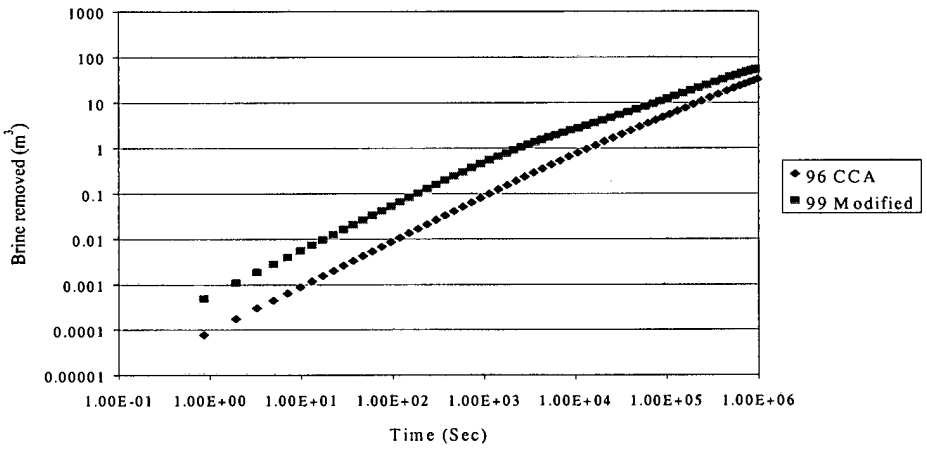

Fig. 6.5 Cumulative brine release vs. time predictions for both the 96 CCA and 99 modified calculations: logarithmic scale. (Down-dip, Replicate 1, Vector 46, Intrusion time 2000 years)

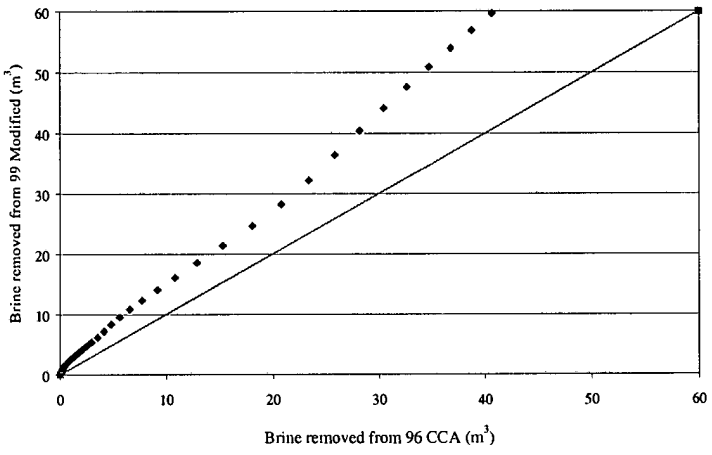

Fig. 6.6 Comparison of cumulative brine release predictions using the 96 CCA and 99 modified calculations. (Down-dip, Replicate 1, Vector 46, Intrusion time 2000 years)

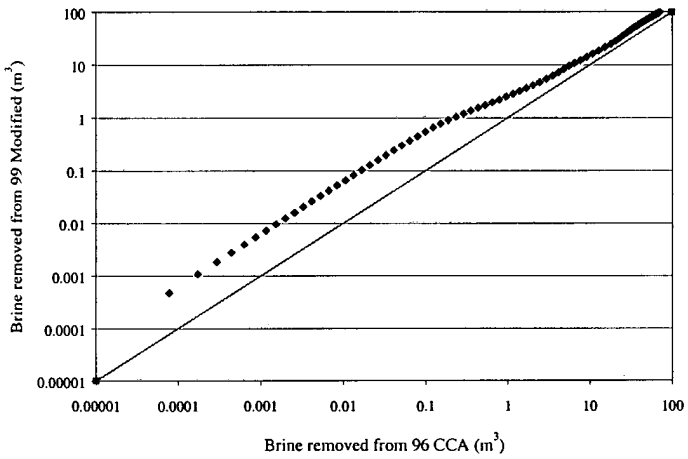

Fig. 6.7 Comparison of cumulative brine release predictions using the 96 CCA and 99 modified calculations: logarithmic scale. (Down-dip, Replicate 1, Vector 46, Intrusion time 2000 years)

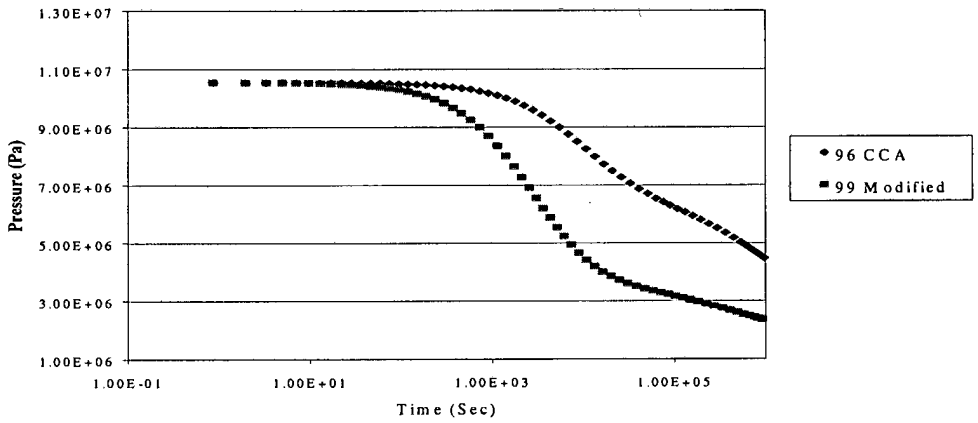

Fig. 6.8 Pressure vs. time predictions in grid block containing intrusion borehole for both the 96 CCA and 99 modified calculations. (Down-dip, Replicate 1, Vector 46, Intrusion time 2000 years)

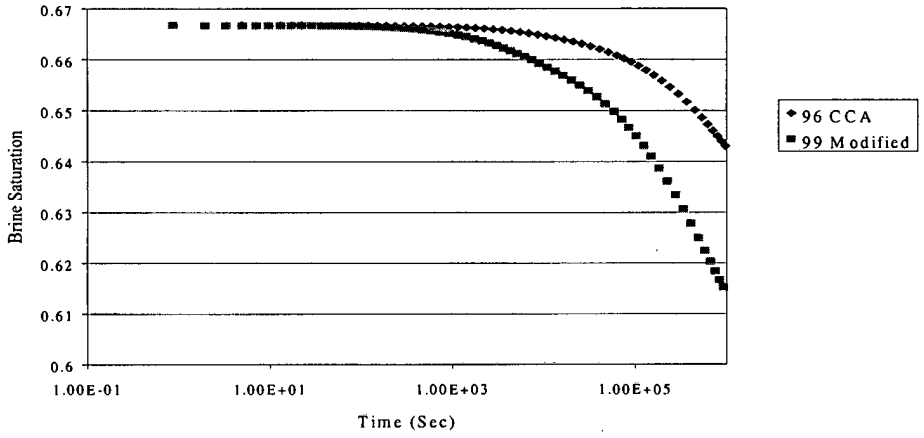

Fig. 6.9 Saturation vs. time predictions in grid block containing intrusion borehole for both the 96 CCA and 99 modified calculations. (Down-dip, Replicate 1, Vector 46, Intrusion time 2000 years)

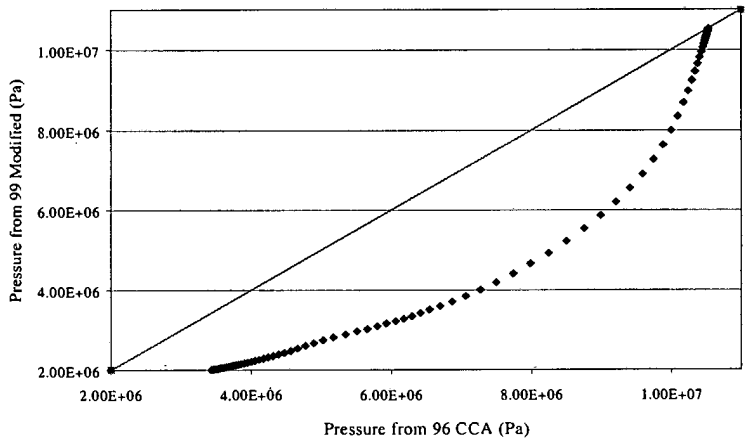

Fig. 6.10 Comparison of pressure predictions in grid block containing intrusion borehole using the 96 CCA and 99 modified calculations. (Down-dip, Replicate 1, Vector 46, Intrusion time 2000 years)

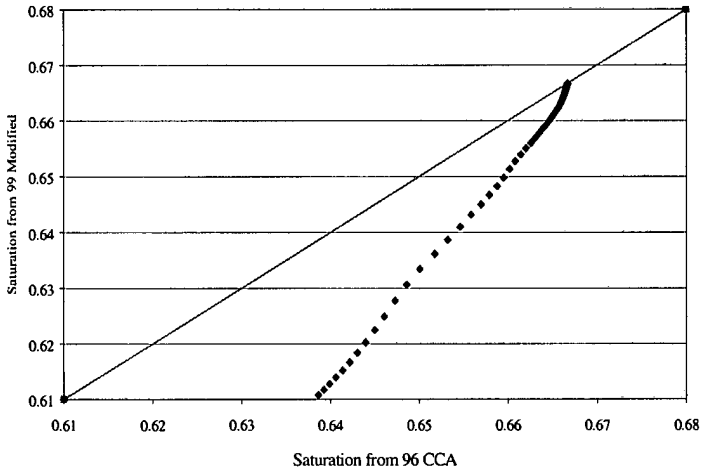

Fig. 6.11 Comparison of saturation predictions in grid block containing intrusion borehole using the 96 CCA and 99 modified calculations. (Down-dip, Replicate 1, Vector 46, Intrusion time 2000 years)

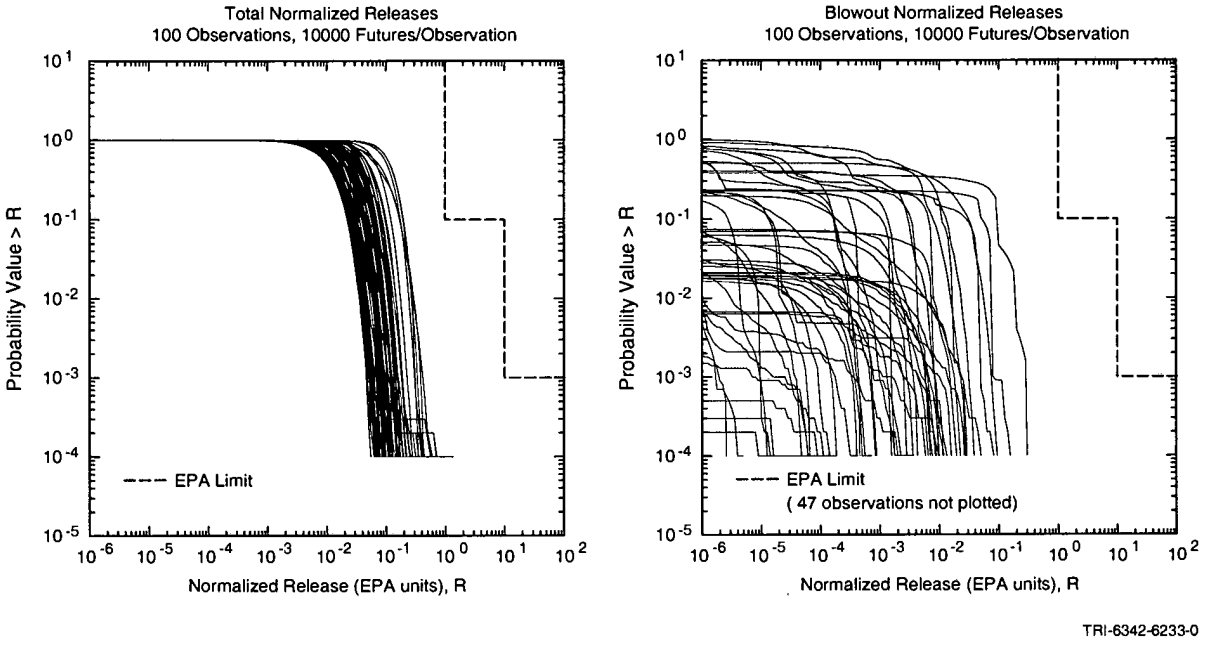

Fig. 6.12 Distribution of CCDFs for normalized release to accessible environment due to total and direct brine releases: new calculations

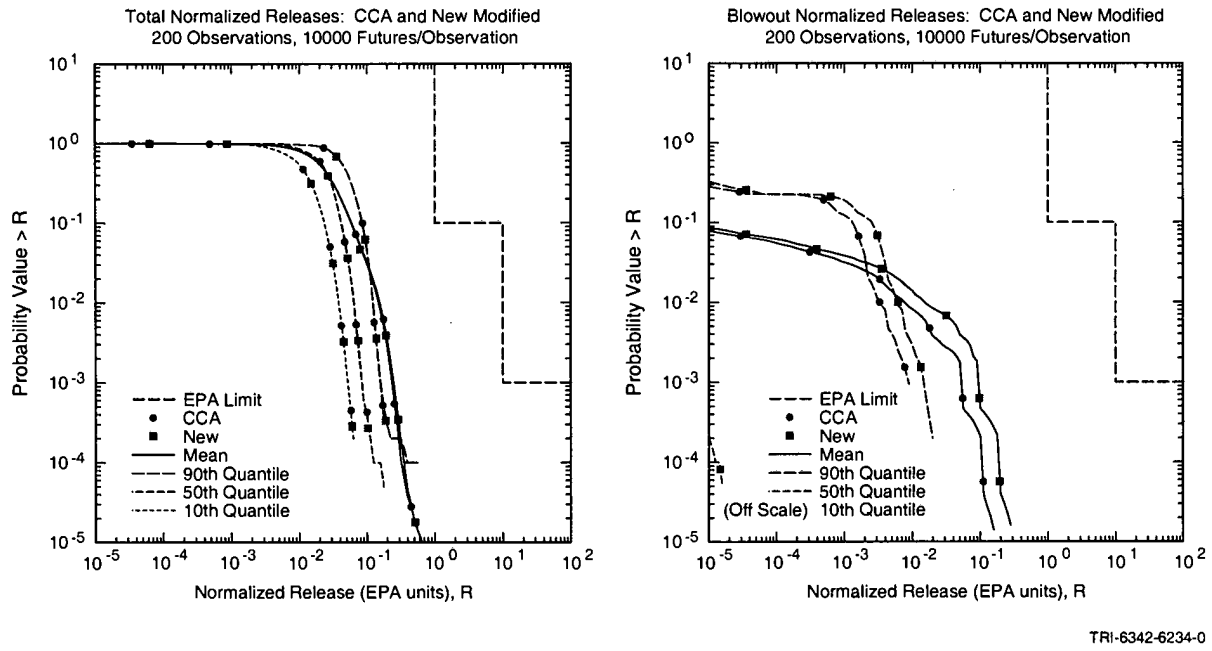

Fig. 6.13 Distribution of CCDFs for normalized release to accessible environment for mean and percentile curves obtained by pooling the replicate: new calculations

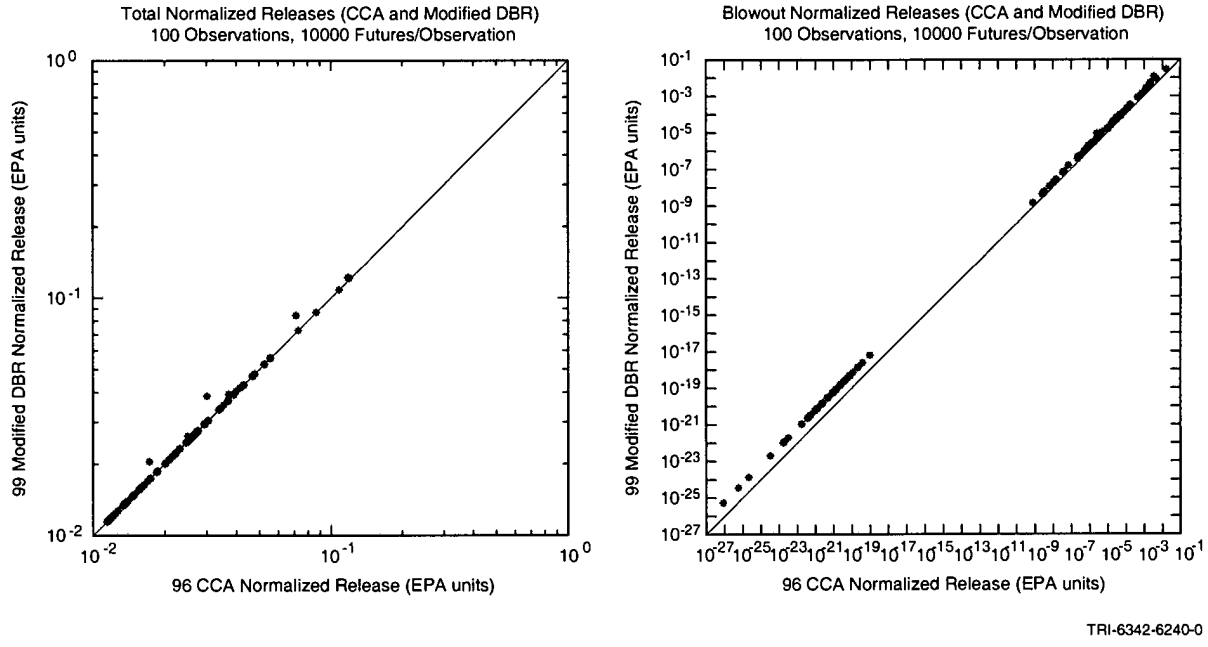

Fig. 6.14 Comparison of distribution of mean CCDFs for normalized release to accessible environment due to total and direct brine releases: 99 modified vs. 96 CCA.

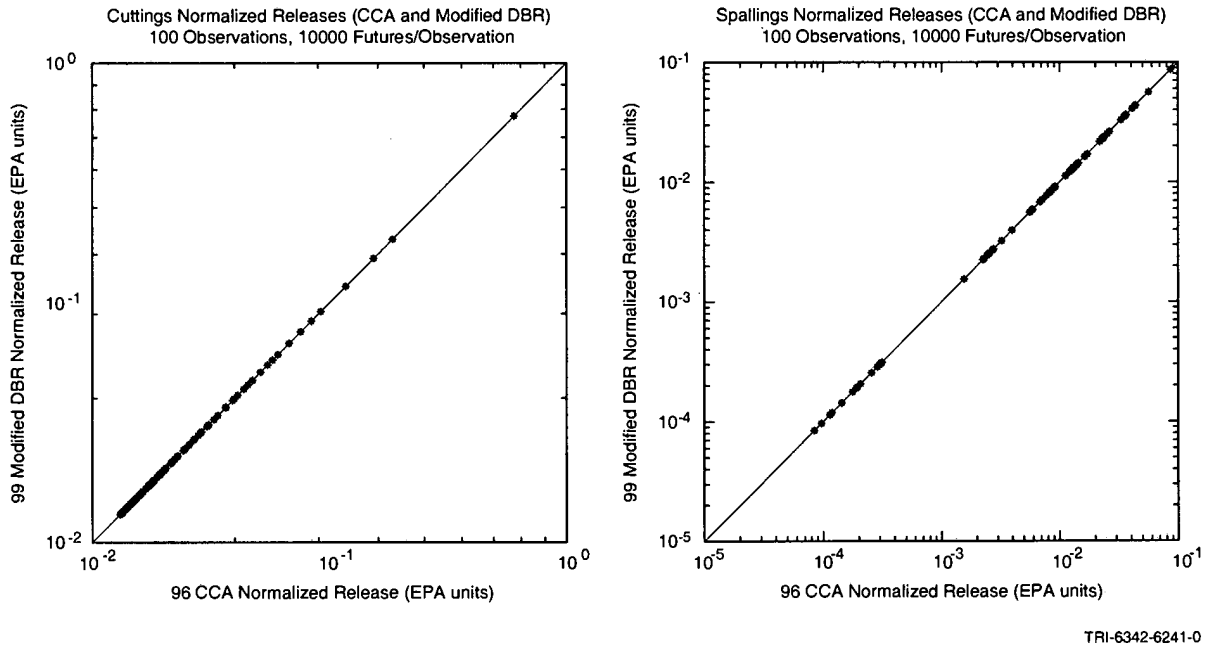

Fig. 6.15 Comparison of distribution of mean CCDFs for normalized release to accessible environment due to cuttings and spallings: 99 modified vs. 96 CCA.

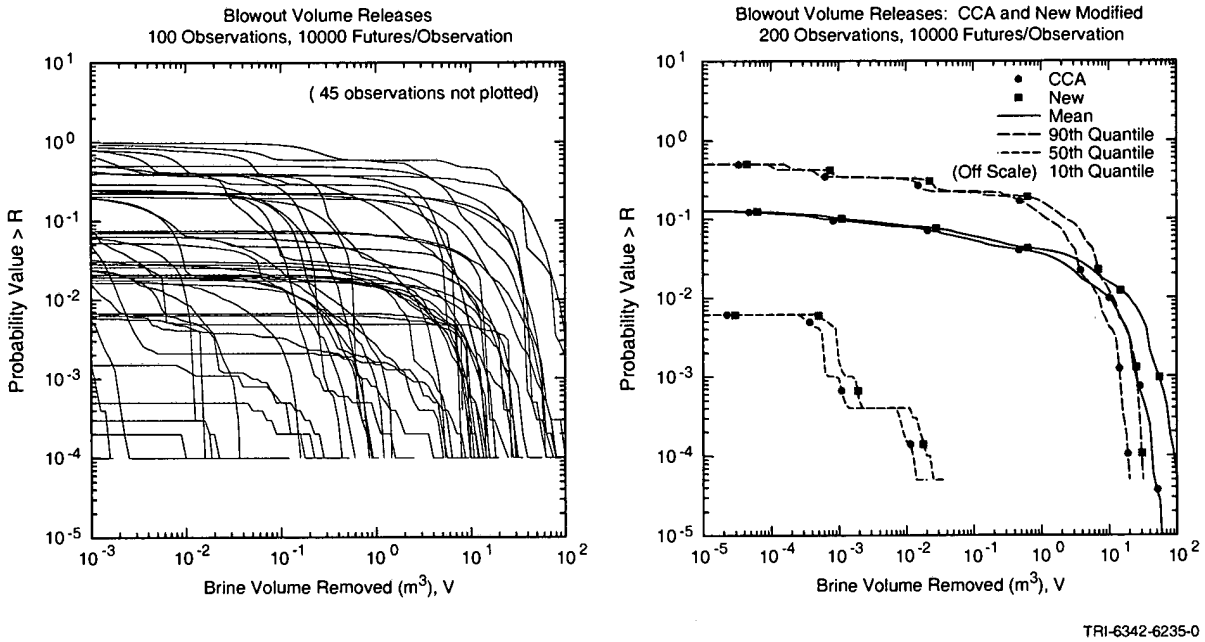

Fig. 6.16 Distribution of CCDFs for volume of brine removed to accessible environment for the replicate and mean and percentile curves: new calculations

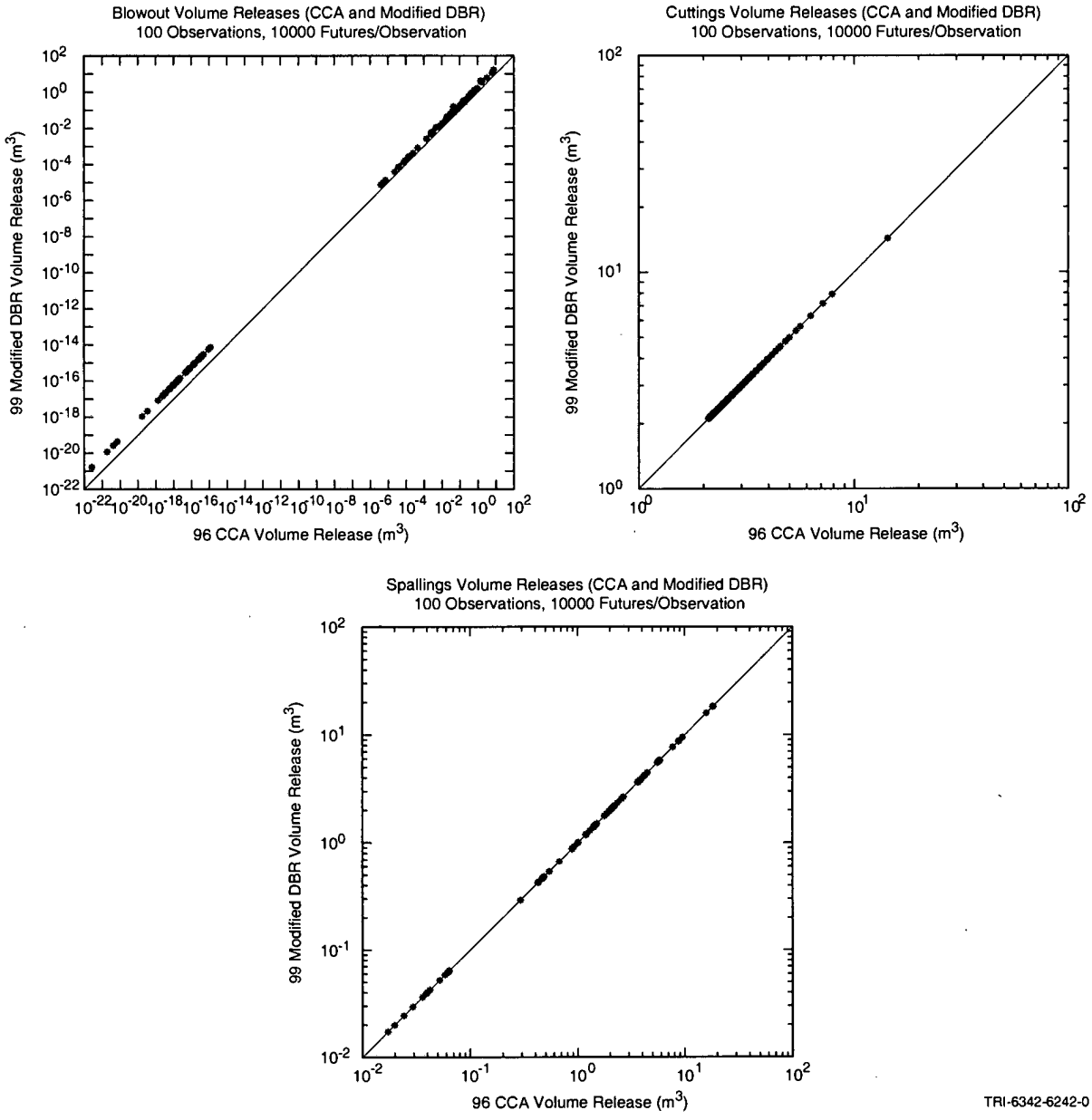

Fig. 6.17 Comparison of distribution of mean CCDFs for volume removed to accessible environment due to direct brine release, cuttings and spallings: 99 modified vs. 96 CCA.

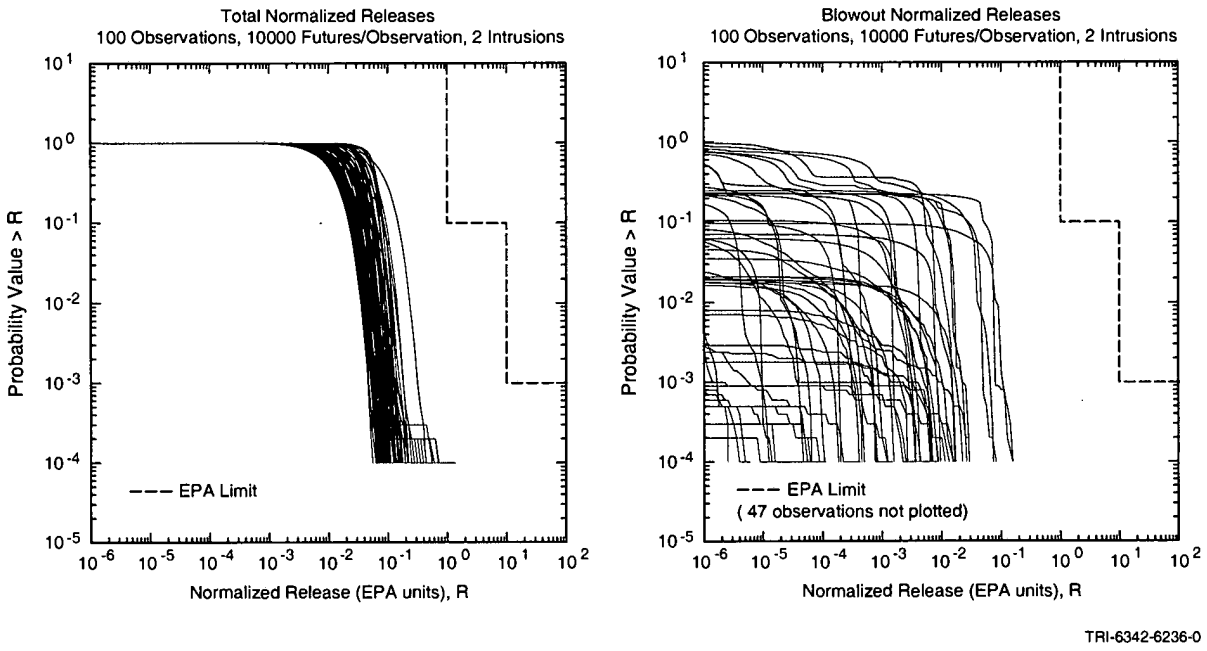

Fig. 6.18 Distribution of CCDFs for normalized release to accessible environment due to total and direct brine releases with the assumption that direct brine releases will only take place for the first two drilling intrusions into the repository: new calculations

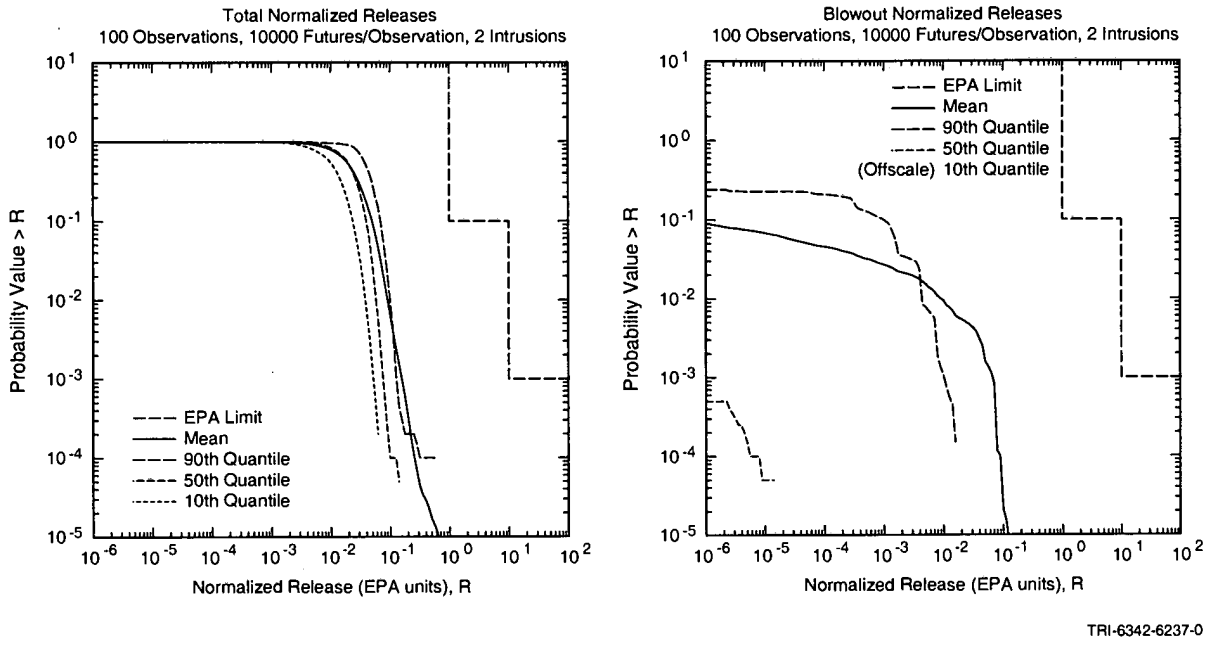

Fig. 6.19 Distribution of CCDFs for normalized release to accessible environment with the assumption that direct brine releases will only take place for the first two drilling intrusions into the repository: CCDFs for mean and percentile curves obtained by pooling the replicate: new calculations

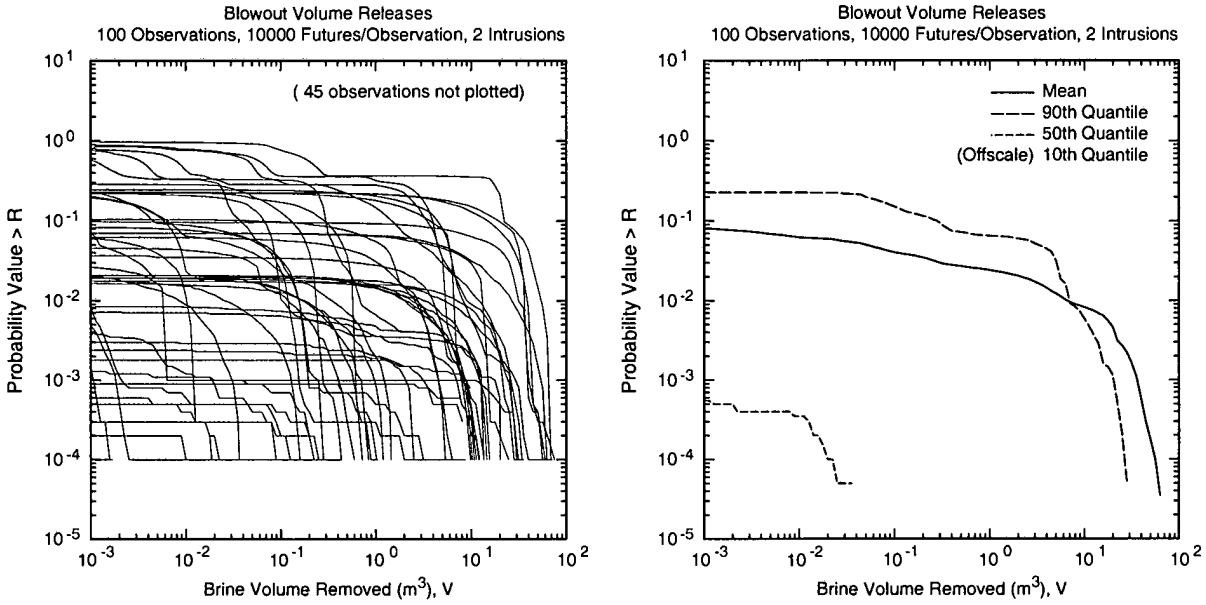

Fig. 6.20 Distribution of CCDFs for volume of brine removed to accessible environment with the assumption that direct brine releases will only take place for the first two drilling intrusions into the repository: CCDFs for total and mean and percentile curves obtained by pooling the replicate: new calculations

8. Conclusion

The objective of this study was to correct the equation of productivity index, to improve the model for abandoned wells, and to report the effect of the modifications on direct brine release predictions of the 1996 CCA. The corrections included multiplying the productivity index by a factor of 2π and using a more descriptive conceptual model for abandoned wells. This involved preparing new curve fits for flowing bottomhole pressure and making corrections in the pre-ALGEBRA input files. In order to formally record the changes made the new calculations were made in CMS. The calculations involved one replicate and five scenarios totaling 5200 calculations. The new direct brine release results were then compared with those of the 1996 CCA. The comparisons show that the amount of brine removed increased by an order of magnitude at low releases, and by about a factor of two for high releases. Since the realizations with high releases are of more importance to the CCDF, such changes did not significantly alter the normalized releases. Use of the new model for abandoned wells did not significantly affect DBR releases.

9. References

Dotson, J. L. (1999) Personal communication.

Hadgu, T., Zimmerman, R. W., and Bodvarsson, G. S. (1995): Coupled Reservoir-Wellbore Simulation of Geothermal Reservoir Behavior, Geothermics, v. 24, no. 2, pp. 145-166.

Helton, J. C., Bean, J. E., Berglund, J. W., Davis, J. F., Economy, K., Garner, J. W., Johnson, J. D., MacKinnon, J. R., Miller, J., O'Brien, G. D., Ramsey, J. L., Schrieber, J. D., Shinta, A., Smith, L. N., Stoelzel, D. M., Stockman, C., and Vaughn, P. (1998): Uncertainty and Sensitivity Analysis Results Obtained in the 1996 Performance Assessment for the Waste Isolation Pilot Plant, Sandia report, SAND98-0365, Albuquerque, NM: Sandia National Laboratories.

Mattax, C. C., and R. L. Dalton (1990): Reservoir Simulation, SPE Monograph 13, Richardson, TX: Henry L. Doherty Memorial Fund Society of Petroleum Engineers Inc.

F. H. Poettmann, and P. G. Carpenter (1952): Multiphase Flow of Gas, Oil, and Water Through Vertical Flow Strings with Application to the Design of Gas-Lift Installations, Drilling and Production Practice, American Petroleum Institute, pp. 257-317.

Stoelzel, D. M., and O'Brien, D. G. (1996): Analysis Package for the BRAGFLO Direct Brine Release Calculations (Task 4) of the Performance Assessment Calculations Supporting Compliance Application (CCA), AP029, Brine Release Calculations, Analysis Package, Albuquerque, NM: Sandia National Laboratories. Sandia WIPP Central Files WPO # 40520.

Williamson, A. S. and Chappelear, J. E. (1981a,b): Representing Wells in Numerical Reservoir Simulation: Part 1 – Theory; Representing Wells in Numerical Reservoir Simulation: Part 2 – Implementation, SPE Journal, v. 21, no. 3, pp. 323-338.